Title
The “lnc” between 3D chromatin structure and X chromosome inactivation

Authors
Pandya-Jones, Amy
Plath, Kathrin

Publication Date
2016-08-01

DOI
10.1016/j.semcdb.2016.04.002

Peer reviewed

Published in final edited form as:

Semin Cell Dev Biol. 2016 August ; 56: 35–47. doi:10.1016/j.semcdb.2016.04.002.

The "lnc" between 3D Chromatin Structure and X Chromosome Inactivation

Amy Pandya-Jones and **Kathrin Plath**

Department of Biological Chemistry, Eli and Edythe Broad Center of Regenerative Medicine and Stem Cell Research, Jonsson Comprehensive Cancer Center, David Geffen School of Medicine at the University of California Los Angeles, Los Angeles, CA 90095, USA

Abstract

The long non-coding RNA *Xist* directs a remarkable instance of developmentally regulated, epigenetic change known as X Chromosome Inactivation (XCI). By spreading *in cis* across the X chromosome from which it is expressed, *Xist* RNA facilities the creation of a heritably silent, heterochromatic nuclear territory that displays a three-dimensional structure distinct from that of the active X chromosome. How *Xist* RNA attaches to and propagates across a chromosome and its influence over the three-dimensional (3D) structure of the inactive X are aspects of XCI that have remained largely unclear. Here, we discuss studies that have made significant contributions towards answering these open questions.

Keywords

X Chromosome Inactivation *Xist*; Chromosome conformation; Non-coding RNA; Heterochromatin

Introduction

X Chromosome Inactivation (XCI) is a critical step in the development of eutherian female organisms. In the mouse, XCI is implemented in two distinct waves during embryogenesis. In a process known as imprinted XCI, the cells of early 2–4 cell stage female conceptuses transcriptionally silence the paternal X chromosome (Xp) such that X-linked gene expression is derived almost exclusively from the maternal X (Xm) chromosome[1–3]. The inactive Xp is then maintained in almost all cells of the developing pre-implantation blastocyst, except for the epiblast cells. These cells, which give rise to the embryo proper, reverse silencing and sustain two transcriptionally active sex chromosomes (XaXa)[4]. Upon implantation, the differentiating epiblast cells transition through a second round of XCI, in which one of the two X chromosomes, this time chosen at random, undergoes transcriptional silencing and facultative heterochromatinization that is heritable throughout all subsequent cell divisions [5–12]. Studies in a variety of model systems have revealed important distinctions in the implementation of both imprinted and random XCI across species [13], making it pertinent to emphasize that in this review, we limit our discussion to that of random XCI.

XCI is attributed with the alignment of X-linked gene dosage in differentiated female cells with that of their male (XY) counterparts [14–16]. Inhibition of XCI in the developing blastocyst affects survival of female embryos and appears to be caused by a failure to instate X-linked gene silencing in the future placenta [17–19]. While this phenotype demonstrates a requirement for imprinted XCI in female embryogenesis, it has hampered efforts to understand whether random XCI is essential for development of the embryo proper, which would require inhibition of XCI specifically in the epiblast but not the trophectoderm cells of an implanting blastocyst. This arrangement of tissue specific control over XCI can be achieved through tetraploid complementation of XCI-deficient epiblast cells, but has not yet been directly tested and as such, the requirement for random XCI in development remains unresolved [20].

The master regulator of XCI is the long non-coding (lnc) RNA *Xist* [21–23]. The *Xist* locus resides upon the X chromosome and is thought to remain inactive throughout the development of male mouse embryos and within the adult male organism [4,17,24–27]. During female development however, *Xist* expression is tightly and dynamically regulated. *Xist* activity becomes detectable in female embryos at the 2–4-cell stage, at which time *Xist* RNA is transcribed solely from the Xp chromosome [13,28,29]. This expression pattern is maintained in cells of the trophectoderm and underlies the imprinted XCI that is observed in these cells and in the extra-embryonic tissues derived from them [30,31]. In later stage pre-implantation embryos, the erasure of imprinted XCI in epiblast cells coincides with a resetting of *Xist* expression, such that the gene appears inactive or is maintained at very low levels of expression [3,13,27,29,31]. As these cells exit from the ‘naïve’ pluripotent state, one of the two *Xist* alleles is upregulated to produce *Xist* transcripts that spread *in cis* along the X chromosome from which they are expressed, thereby forming a ‘coat’ that remains stable throughout the interphase portion of the cell cycle [22,32]. How the upregulation of *Xist* is ensured on only one of the two X chromosomes, chosen at random, is a matter of intense debate. Most models posit that *Xist* activation is promoted by the release of multiple inhibitory pathways acting in the naïve pluripotent state as well as by an increase in *Xist* activators due to induction of differentiation, the details of which have been reviewed elsewhere (see Goodrich et al. in this issue, page XX) [33,34]. Through mechanisms that are still largely unclear, *Xist* RNA initiates the eviction of RNA polymerase II from within the *Xist* RNA coated territory [35,36]. The onset of X-linked gene silencing is accompanied by a temporally sequential deposition of repressive H3K27me3 and H3K9me2 marks, enrichment of the repressive macroH2A histone variant, and DNA methylation on the forming Xi [6,7,11,12,37,38]. Together these and other epigenetic modifications enable the formation and maintenance of a transcriptionally silent, heterochromatic chromosome, known as the inactive X (Xi) [39].

The *Xist* locus remains active specifically on the Xi throughout the somatic lifetime of a cell. Investigations into the requirement of *Xist* post initiation of XCI defined two distinct phases of the process during differentiation. The initiation phase captures the onset of XCI and is characterized by *Xist* RNA-dependent X-linked gene silencing. During this window of time, which generally correlates with the first 72h of differentiation, depletion of *Xist* RNA allows for reactivation of silenced X-linked genes and reverses the XCI program. The maintenance phase follows and is characterized by X-linked gene silencing that is largely

Xist-independent. The loss of *Xist* RNA during this period correlates with the depletion of some enriched heterochromatic marks on the Xi, such as macroH2A and H3K27me3, but extensive reactivation of silenced X-linked genes is not observed [11,39–43].

The *Xist* RNA 'coat' that forms across the Xi has been largely defined by signals observed upon the application RNA Fluorescence In Situ Hybridization (FISH) [44]. Some of the earliest insight into how *Xist* RNA associates with the X chromosome was obtained by treating fixed somatic cells with RNase H, an enzyme that degrades RNA chains involved in RNA:DNA heteroduplexes [32]. RNase H does not act on double- or single-stranded RNAs. When the application of RNase H preceded the hybridization of fluorescent DNA FISH probes to *Xist* RNA, the *Xist* RNA coat over the Xi territory was observed to be intact. This finding suggested that the *Xist* transcripts were not engaged in extensive, if any, RNA:DNA heteroduplexes with genomic DNA. However, to ensure that the *Xist* RNA can indeed bind DNA, the authors also applied RNase H treatment after the DNA probe hybridization step. This reversed order of experimental steps resulted in loss of the FISH signal due to degradation of *Xist* RNA by RNase H and confirmed that, although the *Xist* transcripts are capable of hybridizing to DNA, they do not directly base pair with DNA in the cell. An extension of this conclusion is that *Xist* RNA instead spreads via associations with chromatin and/or the nuclear matrix. In support of this, it has been shown that *Xist* transcripts undergo extensive cis-medicated chromosome spread when expressed from cDNA transgenes integrated at ectopic sites on the X or autosome, or in the context of X:autosomal translocations [41,45–48]. This property of *Xist* was recently exploited in a human pluripotent cell model of Down's Syndrome (trisomy of chromosome 21) [49]. *XIST* expressed from a transgene integrated on one of three chromosome 21's in these cells effectively implemented heritable autosomal inactivation *in cis.* This work not only confirmed that *Xist/XIST* RNA spreads independently of X-linked genomic sequences, but also demonstrated the competence of chromosome 21 to be silenced, while also uncovering a potential therapeutic approach towards the treatment of trisomic disorders that catapulted *Xist* RNA biology into the realm of translational medicine.

In the first half of this review, we will focus on the data that suggest that 3D chromatin conformation determines the spread of *Xist* RNA across the X chromosome. We will also cover the identification of trans-activating factors and the putative roles(s) they play in mediating this process. It has long been appreciated that, once formed, the Xi is structurally distinct from that of the Xa [50]. In the second part of this review, we will address differences in the 3D structure of the Xi in relation to the Xa from cytological, biochemical and genomic perspectives. Our aim is to highlight how the *Xist* RNA*,* by exploiting the 3D architecture of the genome to exert its function also critically impacts genome organization.

Modeling X Chromosome Inactivation *in vitro*

The study of XCI in implanting blastocysts has been limited, at least in part, by their availability, difficulty of genetic manipulation, and low cell number for biochemical analyses. Embryonic stem cells (ESC), derived from epiblast cells of the mouse pre-implantation blastocyst, expand indefinitely in culture and provide an essentially limitless supply of starting material [51,52]. These cells grow clonally, which is convenient for the

isolation of targeted genetic mutants. Like the epiblast cells of the blastocyst, female mouse ESCs maintain two active X chromosomes and upon differentiation, reliably recapitulate the initiation of random XCI [4]. Thus, this *in vitro* system has become a tractable and genetically pliable paradigm for the molecular dissection of XCI. As the findings discussed within this review are based largely upon mouse models of XCI, we provide a short discussion on the benefits and caveats of current mouse cell culture model systems used to study XCI, as this is information that will benefit the understanding of later sections.

Cultured female ESCs are the prevailing model system for the study of random XCI. However, most female ESC lines are unstable with regards to the X chromosome and within a few cell cycles in culture become genetically XO [53]. For reasons that are unclear, genetic stability is retained if the X homologues harbor sufficient distinct single nucleotide polymorphisms (SNP), such as those obtained from an F1 cross of the distantly related C57BL/6 and Cast/Ei strains [54]. This ‘fix’ for stabilization of the XX state in cultured mouse ESCs has become a very useful research tool for studies related to XCI as a means of distinguishing between two otherwise genetically identical chromosomes [27,55,56]. When combined with the complete skewing of XCI, achieved by heterozygous deletion of *Xist* which forces inactivation of the X chromosome housing the intact *Xist* allele, events that occur specifically on the Xi can be mapped using genomics and other approaches [23,56].

An additional consideration of working with a female mouse ESC model system is that the efficiency of differentiation, and thereby the induction of XCI, varies greatly depending on the culture conditions used, and the type of differentiation applied can limit the effective observation of some steps in the XCI process [27]. Moreover, even within a single experiment, the resulting population of fate-restricted cells is typically neither homogenous nor completely synchronous with regards to establishment of XCI. To circumvent these issues, mouse ESC lines with inducible *Xist* cDNA transgenes integrated on the X or on autosomes have been created [46,57]. These ESC lines tend to be male to prevent potential interference from the spontaneous expression of endogenous *Xist* that occurs, albeit at low rates, in female ESC cultures as well as to enable the straightforward identification of epigenetic changes on the single X chromosome. An additional benefit of using male ESCs is that the establishment of XCI results in rather rapid cell death, a phenotype that has been instrumental in defining functional regions of the *Xist* RNA [57]. Establishment of XCI on the targeted chromosome (X or autosome) is presumed to underpin the cell death phenotype. Whether this is due to the silencing of a single locus or of a set of genes crucial for survival has not been determined [57]. It also remains unclear whether XCI in male ESCs transitions beyond the initiation phase prior to cell death and as such, this model system may not be appropriate for studies that interrogate the later steps of XCI.

The recent establishment of haploid ESCs that can be stably propagated in defined media conditions provides a novel model system for the study of XCI that is particularly well suited to assays employing forward genetics [58]. Similar to male cells, induction of XCI on the sole X chromosome in these cells results in cell death and defects in XCI can be uncovered by screening for survival [59]. However, as with male ESCs induced to undergo XCI, this model system is unlikely to offer much insight regarding Xi maintenance and therefore it seems advisable to employ a combination of either haploid or male cells together

with a female model system to fully assess *Xist* RNA mutant phenotypes. The former can synchronously induce *Xist* while also bypassing the complication posed by the stochastic choice of which X becomes inactivated in cells harboring multiple X chromosomes, whereas female ESCs permit studies at all phases of XCI.

3D chromosome conformation directs the initial pattern of Xist RNA spreading

As mentioned above, initial experiments probing the nature of the *Xist* RNA coat implied that it associates with and spreads across chromatin without directly interacting with DNA [32,41,49]. How this is achieved has remained a long-standing question in the field. Efforts to biochemically purify the *Xist* RNA, which is thought to function as a large ribonucleoprotein complex (RNP), have been stymied due to its large size and its tendency to purify with the insoluble components of the nucleus. Consequently, biochemical insight into *Xist* RNA function has remained very limited [60,61]. Fortunately, recent advances in the use of antisense biotinylated oligomers to isolate chromatin-associated RNPs upon crosslinking and fragmentation of chromatin, and the advent of high-throughput DNA sequencing have revolutionized the tractability of *Xist* RNA and have recently been used to define *Xist* RNAs interaction sites on chromatin and to reveal protein factors that both directly and indirectly associate with the *Xist* RNA [36,46,62–65]. Theoretically, the purification of chromatin-associated RNA complexes is straightforward. The various approaches each employ biotinylated oligomers antisense to the RNA of interest, which when applied to lysates from crosslinked cells expressing the transcript of interest, specifically isolate the target RNA with associated chromatin and trans-acting protein factors. However, in practice the approach is not trivial and positive outcomes are largely dependent upon nuances in the optimization of sonication, hybridization, and washing parameters. The general experimental approach and variables that differ between RNA Antisense Purification (RAP), Capture Hybridization Analysis of RNA Targets (CHART), and Chromatin Isolation by RNA Purification (ChIRP) are outlined in Figure 1.

The first successful application of this technology to *Xist* RNA interrogated patterns of *Xist* RNA spread across chromatin during both the initiation and maintenance phases of XCI by RAP-seq (see Pinter. S. in this issue, page XX) [46]. The chromatin contacts of *Xist* RNA in somatic cells, when mapped to the genome at high resolution, revealed an enrichment of X chromosome sequences over autosomal ones. While this outcome was not particularly surprising given the characteristic nature of *Xist* RNA to coat the Xi as revealed by RNA/DNA FISH studies, it confirmed that the *Xist* RNA associates specifically with X-linked chromatin. Notably, *Xist* RNA occupancy was detected across the entirety of the X chromosome in these somatic cells, but accumulated more strongly over regions of high gene density and H3K27me3 enrichment, and less strongly over long interspersed nuclear elements (LINEs). One interpretation of this finding is that although the *Xist* RNA preferentially associates with particular regions of the X, it makes contact with all regions of the X chromosome in all cells during the maintenance phase of XCI. A logical extension of this possibility is that cells must produce sufficient molecules of *Xist* RNA to coat the entirety of the chromosome.

RT-qPCR measurements of *Xist* RNA abundance in different mouse somatic cell types range between 100 and 2000 molecules per cell [66,67]. While this value probably varies with the DNA content of cells and dynamic rates of RNA production and turnover, it seems unlikely that these processes generate the 20-fold difference in RNA abundance reported by the above studies. Whereas the discrepancy is likely most reasonably explained by technical inconsistencies, it may be that cells derived from primary mouse tissues, as performed by Buzin et al., generally express dramatically higher amounts of *Xist* RNA than immortalized MEFs, which were used in experiments by Sunwoo and colleagues. Nevertheless, even the highest of these estimates for *Xist* RNA abundance are much lower than the minimum number of transcripts that would be needed to coat the entirety of the X chromosome, as exemplified by the following, admittedly, overly simplistic scenario. The RAP results require that each basepair of DNA be stoichiometric with at least one RNA nucleotide. To satisfy this condition, almost 9000 17.9kb linear *Xist* transcripts would be needed to tile the 160Mb length of the linear chromosome during the Gap1 phase of the cell cycle. Potentially, these estimates must be doubled during S and Gap2 phases and further increased to account for the observed *Xist* RNA enrichment over most regions of the X. Thus, data on *Xist* RNA abundance instead support an alternative interpretation of the high-resolution chromatin association map of *Xist* RNA, which is that the observed occupancy pattern results from a surprisingly sparse distribution of *Xist* RNA complexes which, rather than coating the entire chromosome, occupy discrete regions of the Xi within individual cells. This more punctuated arrangement of *Xist* RNA on chromatin is observed in high-resolution imaging snapshots of *Xist* RNA FISH in somatic cells, which have shown that the coat is formed from a series of ~50–100 separable RNA foci that decorate the Xi territory [68](Figure 2). Assuming that the *Xist* RNA bound sites differ between cells or if the *Xist* RNA traverses the Xi territory over time, then the resulting *Xist* RNA-associated DNA sequences isolated from a population of cells at steady state may give rise to a similar RAP-seq signature as the one obtained upon interrogation of *Xist* RNA occupancy during the maintenance phase of XCI [68]. It will be important to determine whether the *Xist* RNA foci observed with super resolution microscopy do indeed flux through the Xi or whether they remain statically associated with distinct chromosomal domains that differ between individual cells. Understanding this will entail simultaneous imaging of *Xist* RNA and specific DNA sequences over time using live-imaging microscopy or adapting RAP, CHART or ChIRP to single cells [69,70].

The *de novo* induction of *Xist* in ESCs was leveraged to interrogate the pattern of *Xist* RNA spread during the onset of XCI [46]. By applying RAP to an inducible *Xist* paradigm in male ESCs, whereby *Xist* expression occurs from its endogenous locus, it was demonstrated that, over a time course of hours, the newly expressed *Xist* RNA initially transfers from its transcriptional locus to a set of short (~350kb) regions located distally to its site of transcription, termed early entry sites. An almost identical occupancy signature was observed in female ESCs at a very early (6h) time point of differentiation suggesting that the mechanism of initial spreading is conserved between the two XCI model systems. The early entry sites exhibited no strong enrichment for sequence or specific epigenetic signatures. However, when compared to regions of the genome that are most likely to interact with the *Xist* locus, that is, the sites exhibiting the highest frequency of 3D contacts with the *Xist*

locus as measured by Hi-C conformation capture, a strikingly high correlation between the early entry sites and their 3D proximity to the *Xist* locus was observed [46,71,72]. To determine causality between chromosome conformation and the identity of *Xist* RNA early contact sites, the authors expressed *Xist* from an ectopic site on the X chromosome (*Hprt* locus, 50Mb distal to the *Xist* locus). The 3D conformation of the X chromosome around *Hprt* is different to that observed for *Xist*. Nevertheless, the set of early entry sites identified upon *Xist* RNA expression from the *Hprt* locus remained highly correlated with the genomic regions that contact *Hprt* in 3D. Similar results were obtained when *Xist* was expressed from an autosome [46]. These findings indicated that *Xist* RNA uses a proximity-mediated spreading mechanism to bring it to genomic regions that are closest in 3D distance to the *Xist* locus, even though these sites may be many tens of megabases away when measured linearly along the chromosome. Importantly, the data argue that the pre-existing three-dimensional architecture of the chromosome directs the pattern of *Xist* RNA transfer away from its site of transcription during the onset of XCI (Figure 3).

That *Xist* RNA binds discrete regions specific the X chromosome was also concluded by a later study that characterized spreading at day 3 and 7 post induction of differentiation in female ESCs [65]. The authors reported that the patterns of *Xist* RNA occupancy were highly correlative between these time points and associated with gene rich regions of the chromosome. Interestingly, occupancy of *Xist* RNA over gene poor regions was only noted in MEF cells, suggesting that *Xist* RNA engagement with the X chromosome occurs in several steps and undergoes a transition between differentiating ESCs and the somatic state (MEFs), although the nature of this potential late transition is yet to be determined (see Pinter. S. in this issue, page XX).

A corollary to the proximity-transfer model is the idea that genes proximal to the early entry sites should be silenced faster than those located more distally. Marks and colleagues characterized the dynamics of X-linked gene silencing using RNA-seq over an 8-day time course in differentiating *129/Cast* female ESCs in which XCI was completely skewed towards the *129* homologue [73]. The authors identified four gene clusters corresponding to the degree of silencing that occurred during early (<2 days), intermediate (2–4 days) or late (>4 days) periods within the time course. When mapped to the X chromosome, genes silenced early were, on average, located more closely in linear space to the *Xist* locus than genes within the intermediate cluster. Similarly, genes with late silencing profiles were more distally located relative to *Xist* than those in the intermediate group. By analyzing the data in this manner, the authors argued that the degree of gene silencing over time is dependent, at least in part, on the distance between the gene and the *Xist* locus. However, as Marks et al. observe genes located towards the telomeres that are silenced early as well as many genes located proximal to *Xist* that show a late silencing profile, it is clear that the concentration of *Xist* RNA, as determined via linear spread, is not the sole parameter regulating the dynamics of silencing. While the conclusions by Marks et al. are in seeming contrast to the pattern of silencing expected by a proximity mediated-transfer model, which would predict that genes in closest 3D proximity to early entry sites are silenced fastest, the results may not be as incongruous as they initially appear because 3D contact frequencies are highest closest to the site of interest and decay with increasing linear distance. It will be of interest to correlate the silencing profiles obtained in this study with the *Xist* early entry sites identified by

Engreitz and colleagues to determine whether silencing can also be, at least partially, explained by proximity-mediated transfer. Furthermore, repeating the silencing time course in cells expressing *Xist* from an ectopic locus will greatly help in defining whether these models of *Xist* RNA spreading actually contribute to the timing of gene silencing during the initiation of XCI, as it must also be considered that the mechanisms regulating *Xist* occupancy may be uncoupled from those regulating the dynamics of X-linked gene silencing.

An additional and curious observation regarding the spreading of *Xist* RNA is that, although it does coat the chromosome *in cis* when expressed from an autosomal transgene, the efficiency of coating often appears higher over the X compared to autosomes [41,48]. For this reason, it has been suggested that chromatin on X is more permissive to *Xist* RNA spreading than that of autosomes, but as discussed earlier, *XIST* RNA can implement heritable *bona fide* chromosome silencing of an autosome that is present in triplicate in a cell culture model of Down's syndrome. This discrepancy in *Xist* RNA coating efficiency of the X compared to autosomes may result from increased cell death induced by effective silencing of haploinsufficient genes when *Xist* is expressed from one autosome maintained as a diploid pair, but does not preclude the possibility that differences in 3D genome organization may indeed hamper the equal and effective spread of *Xist* over some, if not all, autosomes. Current evidence suggests that chromosome architecture dictates the initial patterns of *Xist* RNA transfer across a chromosome, but it is not the sole determinant (see below) and it will be important to further our understanding of how chromatin conformation and indeed, epigenetic state, impacts the ability of the *Xist* RNA in particular, and the growing family of chromatin-bound RNAs in general, to find their targets, associate with and spread across chromatin. In the following section, we discuss the data that implicates trans-acting factors in mediating *Xist* RNA's association with chromatin.

Association of *Xist* RNA with chromatin is mediated by protein factors

The molecular parameters that regulate the chromatin association of *Xist* RNA can be assessed via distinct experimental avenues. One approach defines regions of the *Xist* RNA that mediate spreading by experimentally identifying *Xist* mutants that display defects in *Xist* RNA cloud formation or cloud stability. Alternatively, if one assumes that a protein, or set of factors, binds both *Xist* RNA and/or chromatin to tether the two, then it follows that depletion of the factor(s) would similarly disrupt the *Xist* RNA cloud. The prior intractability of the *Xist* RNP made identification of associated protein factors particularly challenging. The recent isolation of the *Xist* RNP has removed this obstacle and much effort in the field is being applied to understanding the functions of the identified proteins in mediating XCI [36,59,63,64,74]. Loss-of-function screens can also provide an alternative approach to uncovering the identity of a factor, and, possibly, its function, if an appropriate phenotype is assessed [59,75].

One predicted characteristic of a protein tether would be the ability to bind nucleic acids. This inductive reasoning was used to pre-select a set of known RNA binding proteins that were targeted in a small scale siRNA screen aimed at identifying factors that interfered with *Xist* RNA cloud integrity in the maintenance phase of XCI [75]. The sole positive result

came from knockdown of SAF-A/hnRNP U (hereafter called SAF-A), a protein that had previously been shown to enrich on the Xi [76][77]. The depletion of SAF-A abrogates *Xist* RNA cloud formation in differentiating female ESCs and effects cloud disintegration in somatic cells, even though *Xist* RNA levels remain stable [36,75]. RT-qPCR analysis of SAF-A immunoprecipitates from UV-treated cells has demonstrated a direct interaction between SAF-A and *Xist* RNA, which has been confirmed through mass spectrometry analysis of proteins isolated from the *Xist* RNP, also under conditions of UV crosslinking [36,75]. SAF-A contains an RGG RNA binding motif as well as a SAF-Box domain that directs binding to AT-rich chromosomal sequences [76,78]. SAF-A mutants lacking either of these nucleic acid binding domains are incapable of rescuing the *Xist* RNA phenotype that is observed upon depletion of SAF-A, indicating that both DNA and RNA binding functions are required to localize *Xist* RNA to chromatin [75]. A recently published CLIP-PCR map of the SAF-A binding sites on *Xist* RNA suggests that SAF-A can bind across the entire *Xist* transcript [79]. The location, size and density of SAF-A binding sites on chromatin remain unknown, but defining them will be important in furthering mechanistic understanding of how SAF-A regulates the chromatin-association of *Xist* transcripts, in particular, and lncRNAs more generally [80].

A second protein implicated in tethering of *Xist* RNA to chromatin is the transcription factor Ying and Yang 1 (YY1). Like SAF-A, knockdown of YY1 does not appear to affect *Xist* RNA levels, but does cause disappearance of the *Xist* RNA cloud in somatic cells [81]. The requirement for YY1 during initiation of XCI is unknown. *Xist* RNA displays little sequence conservation between species. However six distinct repetitive sequences have been identified in both mouse and human homologs [21,82]. The repeats, coined A-F, are each composed of a sequence or set of sequences repeated in tandem, although number of repeated units differs between mouse and human (see the article by Moindrot and Brockdorff in this issue, page XX). YY1 appears to interact with three sites located directly upstream of the F repeat within the genomic *Xist* locus and binds to the C repeat of *Xist* RNA *in vitro*. These findings suggest that YY1 likely nucleates *Xist* at its site of transcription by concerted binding of both DNA and RNA. Whether this nucleic acid co-binding activity is limited to functions at the *Xist* locus or whether YY1 binds across the entire X chromosome to mediate tethering of the RNA at sites distal to *Xist* remains unclear. Additional mechanistic evidence that YY1 can functionally and simultaneously bind both DNA and RNA has recently emerged from work showing that YY1 binds across the genome at active enhancer elements and promoter sequences, where YY1 directly interacts with regulatory RNAs transcribed from these elements [83].

To date, the data on SAF-A and YY1 remain the strongest available evidence for the involvement of trans-acting factors in the association *Xist* RNA to chromatin. As the repertoire of factors that co-bind DNA and RNA increase, so does the likelihood that additional factors will be identified that also mediate *Xist* RNA occupancy on chromatin. As the example of YY1 clearly demonstrates, understanding how these tethers function within the context of XCI will undoubtedly continue to reveal general mechanisms regarding the functional association of RNA at the chromatin interface.

Multiple domains within Xist RNA confer binding to chromatin

The requirement of the *Xist* RNA repeats for initiation of XCI was investigated in an ambitious study, in which inducible *Xist* transgenes, deleted of single or multiple repeats, were integrated upon the X chromosome in male ESCs [57]. As described earlier, induction of wild-type *Xist* resulted in cell death. In screening mutants for survival, the authors uncovered a role for the A-repeat in mediating silencing of X-linked genes. Remarkably, chromosomal coating and *Xist* RNA cloud formation was not grossly affected in the A-repeat (ΔA) mutant cells when assayed by RNA FISH (Wutz et al., 2002). This finding suggested that the *cis*-spreading and transcriptional silencing abilities of the *Xist* RNA are functionally separable and most likely mediated by different domains of the transcript. In accordance with this finding, the general levels of *Xist* RNA occupancy on the X as measured by RAP-seq were also surprisingly similar in cells expressing either wild type or ΔA *Xist* transgenes [46]. However, inspection at higher resolution revealed a two-fold decrease in the localization of ΔA *Xist* RNA over transcriptionally active genes. The first kilobase (kb) of the *Xist RNA* contains the ~350nt A repeat and also binds SHARP/SPEN, a transcriptional repressor required for *Xist* RNA-mediated gene silencing [36,59,63]. Taken together, these data support a model in which SHARP/SPEN binds the *Xist* RNA A repeat to implement transcriptional silencing. However, the RAP-seq result suggests that this RNA domain could confer gene silencing by locally invading regions of active transcription. Uncovering the mechanistic underpinnings regarding how the A-repeat induces transcriptional silencing will require a better understanding of SHARP/SPEN function and as well as a deeper appreciation for the *Xist* domains that facilitate spreading.

The experiments that identified the involvement of the A-repeat in gene silencing also indirectly tested for the minimal *Xist* RNA sequence required to coat the X by assaying for the presence of a of a cloud-like signal FISH signal upon *Xist* expression. It appears that the first ~6kb of the transcript are sufficient to recapitulate the initiation of XCI [57]. Similar findings were obtained in a separate study that made use of female ESCs lacking the *Xist* terminal exon (exon 7) [79]. Whereas wild type *Xist* RNA is 17.9kb in length, differentiation of this mutant line resulted in expression of a stable ~10.2kb transcript. The authors found that the percentage of cells displaying an *Xist* RNA cloud matched that of wild type cells during the early stages of differentiation, but they note a loss of *Xist* RNA clouds in the mutant cells after 8 days of differentiation. The discordance between the observation of a defect in XCI upon deletion of *Xist* exon 7 in female cells but not in the inducible system suggests that the male cells, which undergo cell death after about 48h of *Xist* expression and do not differentiate during this time, do not enter the maintenance phase of XCI and, as such, are incapable of revealing defects in late steps of Xi formation.

An alternative approach to screen for the functional requirement of an RNA element has been the use of Locked Nucleic Acids (LNA) as they display increased hybridization properties that encourage duplex formation and can complement genetic ablation, particularly if the LNA can compete for binding of a trans-acting factor [84]. When LNAs were targeted against the C-repeat of *Xist* RNA in female differentiated cells, detachment of the *Xist* RNA from the X chromosome was observed [85]. The *Xist* RNA cloud remained stable when LNAs against the B, E and F repeats were used, implicating the C-repeat (and a

short 3′ flanking sequence) in tethering of *Xist* RNA to chromatin. These findings regarding *Xist* RNA cloud stability were made in fibroblasts. When the requirement of the *Xist* C-repeat in coating and silencing of the presumptive Xi during the onset of XCI was tested using inducible cDNA transgenes as described above, it was found to be dispensable [57].

The functional demonstration that both the C-repeat and *Xist's* large exon 7 are involved in the upkeep of the *Xist* RNA coat supports a long-standing hypothesis in the field, which is that distinct regions of the *Xist* RNA mediate attachment to chromatin [57]. Furthermore, that the C-repeat and sequences within the terminal exon function during the maintenance phase of XCI but are not apparently essential during the initial spread of the *Xist* RNA, reflect the possibility that the different domains of *Xist* mediate chromatin attachment at distinct stages of XCI. The evidence supporting a requirement of the identified domains in mediating chromatin attachment of *Xist* RNA is based largely on qualitative assessments of the *Xist* RNA cloud integrity as reveled by FISH, which, as an approach, is unlikely to reveal subtle defects in spreading and coating of *Xist* RNA over the Xi. Future experiments regarding the mechanism(s) of *Xist* RNA spread will greatly benefit from the recent development of new technologies like RAP, CHART and ChIRP, that interrogate *Xist* RNA biology at an unprecedented level of resolution and that also provide a more quantitative assessment of RNA spread along chromatin.

In this section, we have attempted to summarize the current state of affairs concerning how *Xist* transcripts tether to and translocate across chromatin. The data generated to date support a model in which *Xist* RNA takes advantage of the 3D genomic landscape to spread across X chromosome to induce formation of the Xi. In the following section, we turn our attention to the question of what happens to the Xi once it has been silenced.

Does the 3D structure of the Xi differ from that of the Xa?

In 1949, Barr and Bertram documented the presence of a nucleolar-associated focus, which they termed a 'nucleolar satellite'. The focus stained strongly with nucleic acid dyes, such as cresyl violet or DAPI, and importantly, was observed in female, but not male, feline neurons [86]. A series of papers published during the following decade reported similar findings in somatic cells from a variety of mammalian tissues, many of which posited that the nucleolar satellite was composed of two female homologous X chromosomes; thereby explaining the absence of the structure in male cells [87–90]. In 1960, Ohno and colleagues invoked the size of the X chromosome, as measured during mitosis, relative to the size of the focus, to perceptively and correctly argue that only a single X chromosome comprised the cytological structure [91,92]. The authors also suggested that the high contrast-staining pattern was due to 'greater compactness' of one X within a diploid nucleus. Through seminal contributions to the XCI field over the past 50 years, primarily by Mary Lyon but also by many others, it is now known that the 'nucleolar satellite' is indeed the somatic Xi or Barr body (Bb) [22,93]. Answers to whether the characteristic, intense staining pattern of the Xi with nucleic acid dyes is due to differences in the compaction of the Xi chromosome compared to its active counterpart (Xa) have been less forthcoming. In the following sections, we consider the cytological and biochemical studies that test the hypothesis that there exist fundamental differences in the chromatin structure of the Xa versus the Xi. We focus on data that assess

3D chromosomal volume, the distance between chromosomal segments and chromosomal contact frequencies, to show that the data support a model in which changes in the large-scale architecture of the X-chromosome, rather than increased compaction of the basic chromatin structure, dictate differences between the Xi and the Xa.

Shape and volume distinguish the Xi from the Xa

Compacted chromatin is thought to adopt a more densely packaged arrangement of nucleosomes than open chromatin and, therefore, would be expected to fill a smaller volume. This logic has been used to predict a smaller nuclear volume for the Xi over the Xa. DNA FISH probes that paint chromosomes have generally been employed to estimate chromosomal volume and through application of this technique, multiple studies using RNA/DNA FISH to identify the *Xist* RNA-coated Xi, have reported that the volume occupied by the Xi is smaller than that of the Xa. Using the total nuclear volume as a normalizer, a standard ratio of between 1.25 +/− 0.05 is consistently reported [55,94,95]. However, to decisively conclude that the nuclear space occupied by the Xi is indeed smaller than that of Xa, the difference between the Xa and Xi should be compared to, and significantly differ from, that between homologous autosomes. By conducting this additional normalization step, Rinke and colleagues showed that the average difference in normalized chromosomal volume between X homologs falls within the range observed for autosome pairs. Thus, rather than being caused by increased compaction, the difference in the volume of the Xi compared to the Xa may simply be due to a natural variation in the nuclear space occupied by homologous chromosomes [95]. Since XCI is random, the authors did not distinguish one X-chromosome homologue from another, thus it remains possible that the Xi is indeed consistently smaller than the Xa and that the chance of an autosome occupying a larger volume than its homologue is instead randomly distributed between the two. To account for this, experiments must test for the *probability* of a difference in the normalized volume between homologous chromosomes, rather than the difference itself. This can be achieved by repeating the measurements of chromosomal volume in polymorphic cells that also harbor a heterozygous *Xist* deletion. This mutation will force inactivation of the chromosome housing the active *Xist* allele and through application of SNP-sensitive FISH to distinguish between individual X chromosomes and autosomes, it may be possible to determine whether the Xi has a higher than average likelihood of being smaller than the Xa relative to autosomes of the same genetic background.

Another experimental consideration in the use of FISH to assess chromosome volume is that, the state of the chromatin may affect the FISH outcome, as compacted chromatin may be less accessible to probe hybridization. Additionally, DNA FISH protocols often, but not necessarily, involve heating and/or dehydration of samples prior to probe hybridization. As these treatments can interfere with 3D chromosome structure, results from these techniques must be interpreted with these caveats in mind [96–98]. The definition of chromosome volume is further compounded by the fact that the boundaries of chromosomal territories are hard to define because they tend to be euchromatic and therefore adopt a more ‘open’ conformation that correlates with an overall weaker, more diffuse fluorescent signal [32,56,99]. This latter factor can impact estimates of chromosome volume because the boundaries of chromosomes are determined by a user-defined thresholding of FISH probe

fluorescence intensity. At lower threshold values, the partial nuclear volume of the Xa is larger than that of the Xi. This pattern inverts at higher cutoffs because a greater percentage of the Xi has, on average, higher fluorescence intensities [99]. The reason for this is likely due to differences in the overall organization of the chromosome, such as denser packaging/compaction of the chromatin or rearrangement of the structure of the Xi. However, this can be tricky to demonstrate because, if chromatin structure influences the intensity of the fluorescent FISH signal, which in turn affects measurements of chromosome volume, then volume cannot be used to estimate compaction as it is itself directly dependent on fluorescence intensity of the FISH signal.

Teller and colleagues tried to address the dependency of volume on fluorescence thresholding by segmenting the chromosome into units of volume (voxels) [99]. The fluorescence was then measured as an intensity value *per voxel*. The mathematical manipulation of segmenting the Xi territory into units of volume introduces an independent parameter that uncouples measurements of total chromosome volume from overall fluorescence intensity. Thus, the integration of the total fluorescence per voxel, over all voxels, when normalized to the total volume of the chromosome, yielded the average signal intensity (ASI), which was used as a proxy for chromatin compaction. The authors report an ASI ratio between the Xi and Xa of 1.2 that is invariant across a range of fluorescence thresholds. It would be convenient to know what the ASI ratio would be if comparing an open euchromatic chromatin state to one that is definitively compacted, such as the chromocenters found in mouse somatic cells. However, in the absence of a comparative scale, the authors conclude that the 20% difference in ASI values between the Xa and Xi suggests only minimal differences in their comparative level of chromatin condensation.

As mentioned above, the notion that the Xi is more compacted than the Xa originated from the observation that the Xi stains more intensely with nucleic acid dyes than the Xa. Smeets and colleagues took advantage of this property to measure chromatin compaction across the X homologs [68]. The authors used DNA FISH on non-dehydrated samples to distinguish X chromosomes from autosomal DNA and then compared the co-localizing DAPI staining pattern to identify the Xi and Xa territories, which were then segmented by DAPI intensity using high-resolution imaging. In this way, the X territories could be described by the percentage of the overall segmented space that falls within a given intensity class, across a distribution of intensity classes. It is important to note that X chromosomes are more AT rich than autosomes. When stained with DAPI, which preferentially binds AT-rich DNA, X chromosomes will fluoresce more intensely. In this instance however, comparing between X chromosomes normalizes for the bias in nucleotide composition. The authors found that a greater proportion of the Xi chromatin, when normalized to the nuclear background and then compared to that of the Xa, contributes to classes representing higher DAPI intensities. This difference was accompanied by a commensurate decrease in the proportion of Xi chromatin within low intensity classes. 3D reconstructions of the DAPI signal revealed a network of low intensity channels throughout the nucleus, which within the Xi territory, were clearly diminished in diameter and invasiveness, suggesting that the overall increase in DAPI staining of the Xi results from a decrease in the inter-chromatin space within the Xi territory.

Apart from volume, the shape of the X chromosomes in somatic cells has also been assessed using both conventional confocal and super-resolution 3D microscopy [94,99]. Interestingly, the Xi appears quite spherical and exhibits a smooth, regular surface. In contrast, the Xa adopts a flatter, ellipsoid-like shape with a larger, more irregular surface (Figure 4). Although the parameter(s) that determine chromosome shape remain unknown, assessing the influence that the *Xist* RNA exerts over the geometry of the Xi would be a very interesting starting point in understanding these differences.

There exist multiple caveats associated with using fluorescence-based approaches to infer relative levels of chromatin compaction and while findings obtained with such techniques must be interpreted with caution, multiple independent studies have concluded that the Xi is, on average, 20% smaller than the Xa, lending credence to the idea that the arrangement of Xi chromatin is distinct from that of the Xa. Furthermore, data from the study by Smeets et al. suggest that this difference may be due to compaction of the inter-chromatin space rather condensation of the basic chromatin structure. We expand upon this idea in the following section with a discussion of cytological and biochemical findings that collectively show that although the basic chromatin structure of the Xi appears similar to that of the Xa, large-scale sub-chromosomal structural differences between the two homologues are observed.

The basic chromatin structure of the Xi is similar that of the Xa

In the nucleus, chromatin is built upon the basic 11nM ‘bead on a string’ fiber, composed of linear DNA wrapped twice around nucleosomes. It is thought that the 11nM fiber then folds into a 30nM fiber which forms the basic structure of chromosomes [100]. The structure, indeed, even the existence of the 30nM fiber *in vivo* is highly debated [101]. *In vitro* however, isolation of chromatin under low salt conditions (5nmM NaCl) yields a 10nM fiber that transitions into a 30nM one with increasing salt (up to 80mM NaCl) [102,103]. Naughton and colleagues used this biochemical property to interrogate the distribution of 30nM chromatin fibers that associate with a more ‘open’ chromatin conformation across the Xi and Xa chromosomes in human somatic lymphoblastoid cells [104][55]. Open chromatin is associated with transcribed and regulatory regions, and as such, is thought to generate 30nM chromatin fibers with disruptions in nucleosome distribution. By this definition, 30nM fibers derived from closed chromatin regions likely display a more regular nucleosomal arrangement. To enrich for sequences associated with a more open structure, the authors separated partially digested chromatin through a sucrose gradient. DNA fragments purified from individual gradient fractions were then size separated by gel electrophoresis. It is assumed that chromatin fragments of similar length and structure will sediment equally though the column. However, fragments of chromatin that adopt a more ‘open’ chromatin structure will sediment more slowly in the gradient than fragments of the same size that are more compact. Thus, DNA sequences isolated from a single gradient fraction that are retarded relative to the bulk upon electrophoresis through a gel, are considered to have originated from regions of more open chromatin. Isolation of these retarded fragments and hybridization to SNP-sensitive microarrays, allowed Naughton et al. to identify the regions of the Xa and Xi that corresponded to a more open conformation. Interestingly, these sites enriched equally (over input) on the Xa as well as the Xi and when mapped back to the X chromosome, the distribution within 1Mb windows across the X was extremely similar. The

authors then focused on Transcription Start Sites (TSS) because these sequences generally associate with open chromatin, and in so doing, found no difference in the abundance of open chromatin at promoters for genes silent on both the Xa and Xi. It must be noted that no observable differences between samples using SNP sensitive arrays may be due to the high failure rate associated with this technique. The hybridization conditions between the probe and its target are determined not only by the SNP but also by the flanking sequence. For this reason, each set of probes targeted against a SNP will have different optimal hybridization parameters and under insufficiently stringent conditions, differences between samples may not be revealed [105]. However, when the authors assessed the TSS's of genes active on the Xa but silent on the Xi, they did observe a two-fold depletion that was limited to the TSS, as no differences were noted at sites upstream or downstream. The notion that the chromatin of the Xi is more compact than the Xa is over 50 years old and it is perhaps surprising that the Xi does not appear generally depleted of open chromatin relative to the Xa, save for small regions encompassing the TSSs of active genes. These findings suggest that differences in the structure of the chromatin fiber between the Xi and Xa, if any, exist at scales larger than that of the 30nM fiber.

Recent work has shown that changes in epigenetic state of chromatin can alter the frequency of interactions between chromosomal segments [106,107]. Given that XCI is associated with large-scale changes in histone modifications on the X chromosome and that little evidence supports changes in the chromatin fiber between the Xi and Xa, it may be that differences in chromatin compaction between the Xa and Xi instead result from rearrangements between sub-chromosomal domains. Teller and colleagues tested this possibility by measuring the linear 3D distance between neighboring segments of the Xa and Xi [99]. To this end, adjacent chromosomal segments were tiled with DNA FISH probes of contrasting colors, and the average inter-segment distances (ISD) were determined. In analyzing four 30–50Mb segments that, when tiled, spanned the length of the X chromosome, the authors found that the 3 ISDs were, on average, 45–68% shorter on the Xi than on the Xa. This corresponds to a contraction in length of approximately 0.5uM – 1.5uM. Similarly, 15 ISDs were measured between sixteen 10Mb segments tiled across the length of the chromosome. In this case, only 4 ISDs exhibited any significant difference in length between the two X homologs and of these, the ISD with the largest length differential encompassed the centromere. To determine whether shortening of ISDs at the 10Mb scale translated to detectable differences at smaller distances, the authors further segmented two of the four 10Mb domains that displayed differential ISDs, but found no significant change between the two X chromosomes at the 1Mb scale. In a separate study using a highly similar method, ISD length measurements at the sub-megabase scale did not reveal any differences between the Xa and Xi except for a 1.5 fold increase in ISD contraction on the Xi relative to the Xa between gene-rich regions [55]. To summarize these data, it appears that the greatest contraction in inter-segment distances observed between identical regions of the Xa versus the Xi occur over large 30–50Mb sub-chromosomal domains. Smaller scale contractions around the centromere are also observed at 10Mb scale, with only significant reductions in ISD length at the 0.5 – 4Mb scale in regions with high gene density (Figure 4).

The conclusions drawn from the above observations are largely supported by data obtained by electron microscopy (EM), which has shown that the Xi chromatin folds into largely

independent domains that are each 60–300nM in diameter and are separated by channels of up to 400nM in width, that appear contiguous with the surrounding nucleoplasm [68,108]. That the contraction in ISDs at the 30+Mb scale accompanies an absence of change at smaller genomic distances coupled with the observation that the Xi chromatin appears to adopt a higher order folding pattern by EM inspection, suggests a model in which segments of the X coalesce into larger domains during formation of the Xi and it is these alterations in the overall 3D architecture of the chromosome, rather than compaction of the basic chromatin fibers, that define the distinct genomic conformation of the Xi. In the following and final section, we explore the findings that have emerged from the application of Chromosome Conformation Capture techniques to study the 3D organization of the X Chromosome.

The Xi forms a bipartite structure with 3D contacts that differ from the Xa

The advent of high throughput sequencing coupled with the development of Chromosome Conformation Capture (3C) techniques has made it possible to probe the frequency with which any one DNA sequence contacts all other genomic sites across the genome of a cell [109]. These novel applications provide an independent method for probing genome organization, and have revealed that regions of open, or more transcriptionally active, chromatin self-associate to form what has been termed the ‘A’ compartment whereas closed, more transcriptionally silent regions form the ‘B’ compartment. Within each of these compartments, chromosomes are organized into topologically associating domains that range in size from 40kb to 3Mb across the genome and appear to be conserved across cell types [71,72,107].

Conformation capture techniques have been applied to understanding the changes in contacts made by genes on the Xi relative to those on its active counterpart. Taking advantage of X-linked polymorphisms and skewing of XCI through deletion of *Xist*, Splinter and colleagues have demonstrated that active genes on the Xa show a propensity to interact with other active regions, both *in cis* and *in trans* [56]. On the Xi, active genes that escape XCI, such as Jarid1C, form contacts with other escapee loci. However, analysis of the genes subject to silencing on the Xi that on the Xa engage in multiple long-range contacts, show a remarkably stunted repertoire of contacts on the Xi [56,107,110,111]. While incomplete digestion of heterochromatic Xi chromatin may account for this observation, the more interesting possibility is that the attenuation of specific intra-chromosomal contacts between silenced loci on the Xi results from modifications to its overall architecture, which would be in accordance with the findings described above by Teller and colleagues [99].

Furthering this line of inquiry, two groups used Hi-C technology to characterize all possible contacts made by the Xa and Xi at 100kb or better resolution. Both groups reported that Xi contact points are segregated into two large superdomains [107,110]. The contact map is surprisingly consistent across a panel human and mouse cells, the latter of which were harvested from both *in vitro* and *in vivo* growth conditions that are representative of different developmental stages. The invariance in the observed long-range contact frequencies suggests that the unique genomic architecture of the Xi forms in an ordered manner that is consistent between cell types and across species.

Predictive 3D modeling of the Hi-C data depicts the Xi as a bipartite structure composed of two arms that each exhibit a large degree of spatial separation [110]. Each arm represents a single HiC superdomain. It is interesting that the bipartite structure was noted by Ohno and Hauschka over 50 years ago, who, regarding the appearance of the Xi in their chromatin spreads from mouse cells, wrote: “Indeed, the sex chromatin often seems clearly bipartite… [and]….results from the tendency of a single heteropyknotic X to fold at the middle” [91]. It turns out that at the two arms are separated by a hinge/boundary region, which in both mouse and humans is located proximal to the *DXZ4/Dxz4* locus [107,110]. In humans, *DXZ4* is located within the Xq23 band, 74.6kb upstream of the Plastin gene and 296.5Kb downstream of the angiotensin II receptor locus (*AGTR2).* This macrosatellite repeat is composed of 12–100 3kb repeating units that are heterochomatinized on the X in males and on the Xa in females [112]. On the Xi, however, this repeat region is packaged into euchromatin and is bound by the factors CTCF and YY1 [110,113]. CTCF is an essential protein that functions as a versatile transcriptional regulator, but recently has been characterized as playing a major role in the organization of chromatin [114]. The *DXZ4* locus generates an RNA that is expressed on both the Xa and Xi from a bi-directional promoter located within each repeat [115]. The *DXZ4* locus also forms two long-range interactions with other euchromatic, CTCF-bound repetitive sites on the Xi. These regions are located at 58Mb proximal to and 132Mb distal to the *DXZ4* locus and are also actively transcribed [107,113]. An additional 25 Xi-specific long-range (7–74Mb) interactions were identified, for which the anchor sequences for three of them encode the non-coding RNAs *XIST, FIRRE* and *Loc550643* [107]. Although the functional significance of these long range interactions remains unclear, it is curious that, in the absence of *Xist*, genes on the Xi that remain silenced re-initiate contacts similar to those found for the homologous alleles on the Xa [56]. It will be interesting to test whether similar changes in contact frequencies are observed upon loss of *FIRRE/Firre, DXZ4/Dxz4* and *Loc550643*, the results of which may reveal insight into how lncRNAs in general, and XCI-related ones in particular, influence genome architecture.

In this second section, we have tried to succinctly summarize the data from a very large body of work regarding the structure of the Xi and how it is distinguished from the Xa. While the available data does not strongly support increased condensation of the chromatin fiber comprising the Xi, it seems clear that there are differences in the shape and overall architecture of the Xi compared to the Xa that, importantly, can now be quantified with novel high-resolution imaging and high-throughput sequencing techniques. Why these differences exist remains unclear and future work in this area will hopefully uncover causal link(s) between these parameters and the maintenance of the silent state of the Xi.

Towards a comprehensive understanding of *Xist* RNA function

A quarter century of research on *Xist* RNA biology has detailed how upregulated expression of *Xist* during embryogenesis results in coating of the presumptive Xi by the *Xist* RNA and heterochromatinization of the chromosome, to ultimately lock in a heritable, transcriptionally silenced state. To achieve this remarkable feat, the *Xist* RNA exploits and also shapes chromosome conformation by directly preventing contacts between sites on the X or through indirect alteration of the linear chromatin character. Much of the work that

uncovered these functions of *Xist* RNA remains pioneering and seminal, not only within the XCI field but also for the fields of epigenetic regulation of gene expression and lncRNA biology. Yet, for all of the discoveries that have been made, the length of the *Xist* RNA coupled with its requirement for chromatin attachment has severely hindered its *in vitro* tractability and has stunted the advancement of mechanistic insight regarding how the *Xist* RNP functions. Recent advances in novel technologies that permit directed genome editing *in vivo* (CRISPR), the characterization of global chromatin structure (Hi-C), the comprehensive elucidation RNA-chromatin contacts (RAP/CHART/ChIRP), as well the production of genome-wide nucleic acid-protein interaction maps (ChIP, CLIP, RAP-MS, CHiRP-MS, DRiP and similar methods) promise a fascinating and data-rich avenue of research, by which the mechanisms of *Xist* RNA function can be probed *in vivo* at an unprecedented level of detail across many different developmental stages. While much work remains, there is no doubt that the future of *Xist* RNA research is bright and will continue to illuminate the world of lncRNA biology.

Acknowledgments

We are grateful to Dr. Yolanda Markaki for providing 3D-SIM images. Our work is supported through funds from the UCLA Eli and Edythe Broad Center of Regenerative Medicine and Stem Cell Research, the UCLA David Geffen School of Medicine, CIRM, and NIH P01 GM099134 (to KP), and NIH F32 GM103139-01 NRSA and Helen Hay Whitney postdoctoral fellowships (to AP-J). We sincerely apologize to colleagues whose work we were unable to discuss due to space limitations.

References cited

1. Monk M, Harper MI. Sequential X chromosome inactivation coupled with cellular differentiation in early mouse embryos. Nature. 1979; 281:311–313. [PubMed: 551278]
2. Takagi N, Sasaki M. Preferential inactivation of the paternally derived X chromosome in the extraembryonic membranes of the mouse. Nature. 1975; 256:640–642. [PubMed: 1152998]
3. Williams LH, Kalantry S, Starmer J, Magnuson T. Transcription precedes loss of Xist coating and depletion of H3K27me3 during X-chromosome reprogramming in the mouse inner cell mass. Dev Camb Engl. 2011; 138:2049–2057. DOI: 10.1242/dev.061176
4. Kay GF, Penny GD, Patel D, Ashworth A, Brockdorff N, Rastan S. Expression of Xist during mouse development suggests a role in the initiation of X chromosome inactivation. Cell. 1993; 72:171–182. [PubMed: 8425217]
5. Beutler E, Yeh M, Fairbanks VF. The normal human female as a mosaic of X-chromosome activity: studies using the gene for C-6-PD-deficiency as a marker. Proc Natl Acad Sci U S A. 1962; 48:9–16. [PubMed: 13868717]
6. Costanzi C, Pehrson JR. Histone macroH2A1 is concentrated in the inactive X chromosome of female mammals. Nature. 1998; 393:599–601. DOI: 10.1038/31275 [PubMed: 9634239]
7. Gendrel A-V, Apedaile A, Coker H, Termanis A, Zvetkova I, Godwin J, et al. Smchd1-dependent and -independent pathways determine developmental dynamics of CpG island methylation on the inactive X chromosome. Dev Cell. 2012; 23:265–279. DOI: 10.1016/j.devcel.2012.06.011 [PubMed: 22841499]
8. Heard E, Rougeulle C, Arnaud D, Avner P, Allis CD, Spector DL. Methylation of histone H3 at Lys-9 is an early mark on the X chromosome during X inactivation. Cell. 2001; 107:727–738. [PubMed: 11747809]
9. Mermoud JE, Costanzi C, Pehrson JR, Brockdorff N. Histone macroH2A1.2 relocates to the inactive X chromosome after initiation and propagation of X-inactivation. J Cell Biol. 1999; 147:1399–1408. [PubMed: 10613899]

10. de Napoles M, Mermoud JE, Wakao R, Tang YA, Endoh M, Appanah R, et al. Polycomb group proteins Ring1A/B link ubiquitylation of histone H2A to heritable gene silencing and X inactivation. Dev Cell. 2004; 7:663–676. DOI: 10.1016/j.devcel.2004.10.005 [PubMed: 15525528]
11. Plath K, Fang J, Mlynarczyk-Evans SK, Cao R, Worringer KA, Wang H, et al. Role of histone H3 lysine 27 methylation in X inactivation. Science. 2003; 300:131–135. DOI: 10.1126/science.1084274 [PubMed: 12649488]
12. Silva J, Mak W, Zvetkova I, Appanah R, Nesterova TB, Webster Z, et al. Establishment of histone h3 methylation on the inactive X chromosome requires transient recruitment of Eed-Enx1 polycomb group complexes. Dev Cell. 2003; 4:481–495. [PubMed: 12689588]
13. Okamoto I, Patrat C, Thépot D, Peynot N, Fauque P, Daniel N, et al. Eutherian mammals use diverse strategies to initiate X-chromosome inactivation during development. Nature. 2011; 472:370–374. DOI: 10.1038/nature09872 [PubMed: 21471966]
14. Frota-Pessoa O, Gomes EL, Calicchio TR. Christmas factor: dosage compensation and the production of blood coagulation factor IX. Science. 1963; 139:348–349. [PubMed: 13945845]
15. Gardner RL, Lyon MF. X chromosome inactivation studied by injection of a single cell into the mouse blastocyst. Nature. 1971; 231:385–386. [PubMed: 4931003]
16. Monk M, Kathuria H. Dosage compensation for an X-linked gene in pre-implantation mouse embryos. Nature. 1977; 270:599–601. [PubMed: 563522]
17. Marahrens Y, Panning B, Dausman J, Strauss W, Jaenisch R. Xist-deficient mice are defective in dosage compensation but not spermatogenesis. Genes Dev. 1997; 11:156–166. [PubMed: 9009199]
18. Mugford JW, Yee D, Magnuson T. Failure of extra-embryonic progenitor maintenance in the absence of dosage compensation. Dev Camb Engl. 2012; 139:2130–2138. DOI: 10.1242/dev.076497
19. Takagi N. Primary and secondary nonrandom X chromosome inactivation in early female mouse embryos carrying Searle's translocation T(X; 16)16H. Chromosoma. 1980; 81:439–459. [PubMed: 7449570]
20. Tam PPL. Mouse embryonic chimeras: tools for studying mammalian development. Development. 2003; 130:6155–6163. DOI: 10.1242/dev.00893 [PubMed: 14623817]
21. Brockdorff N, Ashworth A, Kay GF, McCabe VM, Norris DP, Cooper PJ, et al. The product of the mouse Xist gene is a 15 kb inactive X-specific transcript containing no conserved ORF and located in the nucleus. Cell. 1992; 71:515–526. [PubMed: 1423610]
22. Brown CJ, Hendrich BD, Rupert JL, Lafrenière RG, Xing Y, Lawrence J, et al. The human XIST gene: analysis of a 17 kb inactive X-specific RNA that contains conserved repeats and is highly localized within the nucleus. Cell. 1992; 71:527–542. [PubMed: 1423611]
23. Penny GD, Kay GF, Sheardown SA, Rastan S, Brockdorff N. Requirement for Xist in X chromosome inactivation. Nature. 1996; 379:131–137. DOI: 10.1038/379131a0 [PubMed: 8538762]
24. Borsani G, Tonlorenzi R, Simmler MC, Dandolo L, Arnaud D, Capra V, et al. Characterization of a murine gene expressed from the inactive X chromosome. Nature. 1991; 351:325–329. DOI: 10.1038/351325a0 [PubMed: 2034278]
25. Brockdorff N, Ashworth A, Kay GF, Cooper P, Smith S, McCabe VM, et al. Conservation of position and exclusive expression of mouse Xist from the inactive X chromosome. Nature. 1991; 351:329–331. DOI: 10.1038/351329a0 [PubMed: 2034279]
26. Brown CJ, Ballabio A, Rupert JL, Lafreniere RG, Grompe M, Tonlorenzi R, et al. A gene from the region of the human X inactivation centre is expressed exclusively from the inactive X chromosome. Nature. 1991; 349:38–44. DOI: 10.1038/349038a0 [PubMed: 1985261]
27. Gayen S, Maclary E, Buttigieg E, Hinten M, Kalantry S. A Primary Role for the Tsix lncRNA in Maintaining Random X-Chromosome Inactivation. Cell Rep. 2015; 11:1251–1265. DOI: 10.1016/j.celrep.2015.04.039 [PubMed: 25981039]
28. Hartshorn C, Rice JE, Wangh LJ. Developmentally-regulated changes of Xist RNA levels in single preimplantation mouse embryos, as revealed by quantitative real-time PCR. Mol Reprod Dev. 2002; 61:425–436. DOI: 10.1002/mrd.10037 [PubMed: 11891913]

29. Nesterova TB, Barton SC, Surani MA, Brockdorff N. Loss of Xist imprinting in diploid parthenogenetic preimplantation embryos. Dev Biol. 2001; 235:343–350. DOI: 10.1006/dbio.2001.0295 [PubMed: 11437441]
30. Corbel C, Diabangouaya P, Gendrel A-V, Chow JC, Heard E. Unusual chromatin status and organization of the inactive X chromosome in murine trophoblast giant cells. Dev Camb Engl. 2013; 140:861–872. DOI: 10.1242/dev.087429
31. Mak W. Reactivation of the Paternal X Chromosome in Early Mouse Embryos. Science. 2004; 303:666–669. DOI: 10.1126/science.1092674 [PubMed: 14752160]
32. Clemson CM, McNeil JA, Willard HF, Lawrence JB. XIST RNA paints the inactive X chromosome at interphase: evidence for a novel RNA involved in nuclear/chromosome structure. J Cell Biol. 1996; 132:259–275. [PubMed: 8636206]
33. van Bemmel JG, Mira-Bontenbal H, Gribnau J. Cis- and trans-regulation in X inactivation. Chromosoma. 2016; 125:41–50. DOI: 10.1007/s00412-015-0525-x [PubMed: 26198462]
34. Galupa R, Heard E. X-chromosome inactivation: new insights into cis and trans regulation. Curr Opin Genet Dev. 2015; 31:57–66. DOI: 10.1016/j.gde.2015.04.002 [PubMed: 26004255]
35. Chaumeil J, Le Baccon P, Wutz A, Heard E. A novel role for Xist RNA in the formation of a repressive nuclear compartment into which genes are recruited when silenced. Genes Dev. 2006; 20:2223–2237. DOI: 10.1101/gad.380906 [PubMed: 16912274]
36. McHugh CA, Chen C-K, Chow A, Surka CF, Tran C, McDonel P, et al. The Xist lncRNA interacts directly with SHARP to silence transcription through HDAC3. Nature. 2015; 521:232–236. DOI: 10.1038/nature14443 [PubMed: 25915022]
37. Escamilla-Del-Arenal M, da Rocha ST, Spruijt CG, Masui O, Renaud O, Smits AH, et al. Cdyl, a new partner of the inactive X chromosome and potential reader of H3K27me3 and H3K9me2. Mol Cell Biol. 2013; 33:5005–5020. DOI: 10.1128/MCB.00866-13 [PubMed: 24144980]
38. Rougeulle C, Chaumeil J, Sarma K, Allis CD, Reinberg D, Avner P, et al. Differential histone H3 Lys-9 and Lys-27 methylation profiles on the X chromosome. Mol Cell Biol. 2004; 24:5475–5484. DOI: 10.1128/MCB.24.12.5475-5484.2004 [PubMed: 15169908]
39. Csankovszki G, Panning B, Bates B, Pehrson JR, Jaenisch R. Conditional deletion of Xist disrupts histone macroH2A localization but not maintenance of X inactivation. Nat Genet. 1999; 22:323–324. DOI: 10.1038/11887 [PubMed: 10431231]
40. Csankovszki G, Nagy A, Jaenisch R. Synergism of Xist RNA, DNA methylation, and histone hypoacetylation in maintaining X chromosome inactivation. J Cell Biol. 2001; 153:773–784. [PubMed: 11352938]
41. Wutz A, Jaenisch R. A shift from reversible to irreversible X inactivation is triggered during ES cell differentiation. Mol Cell. 2000; 5:695–705. [PubMed: 10882105]
42. Yildirim E, Kirby JE, Brown DE, Mercier FE, Sadreyev RI, Scadden DT, et al. Xist RNA is a potent suppressor of hematologic cancer in mice. Cell. 2013; 152:727–742. DOI: 10.1016/j.cell.2013.01.034 [PubMed: 23415223]
43. Zhang L-F, Huynh KD, Lee JT. Perinucleolar targeting of the inactive X during S phase: evidence for a role in the maintenance of silencing. Cell. 2007; 129:693–706. DOI: 10.1016/j.cell.2007.03.036 [PubMed: 17512404]
44. Brown CJ, Hendrich BD, Rupert JL, Lafrenière RG, Xing Y, Lawrence J, et al. The human XIST gene: analysis of a 17 kb inactive X-specific RNA that contains conserved repeats and is highly localized within the nucleus. Cell. 1992; 71:527–542. [PubMed: 1423611]
45. Allderdice PW, Miller OJ, Miller DA, Klinger HP, Opitz JM. Spreading of inactivation in an (X;14) translocation. Am J Med Genet. 1978; 2:233–240. DOI: 10.1002/ajmg.1320020304 [PubMed: 263441]
46. Engreitz JM, Pandya-Jones A, McDonel P, Shishkin A, Sirokman K, Surka C, et al. The Xist lncRNA exploits three-dimensional genome architecture to spread across the X chromosome. Science. 2013; 341:1237973.doi: 10.1126/science.1237973 [PubMed: 23828888]
47. Lee JT, Strauss WM, Dausman JA, Jaenisch R. A 450 kb transgene displays properties of the mammalian X-inactivation center. Cell. 1996; 86:83–94. [PubMed: 8689690]

48. Popova BC, Tada T, Takagi N, Brockdorff N, Nesterova TB. Attenuated spread of X-inactivation in an X;autosome translocation. Proc Natl Acad Sci U S A. 2006; 103:7706–7711. DOI: 10.1073/pnas.0602021103 [PubMed: 16679409]
49. Jiang J, Jing Y, Cost GJ, Chiang J-C, Kolpa HJ, Cotton AM, et al. Translating dosage compensation to trisomy 21. Nature. 2013; 500:296–300. DOI: 10.1038/nature12394 [PubMed: 23863942]
50. Ohno S, Kaplan WD, Kinosita R. Formation of the sex chromatin by a single X-chromosome in liver cells of Rattus norvegicus. Exp Cell Res. 1959; 18:415–418. [PubMed: 14428474]
51. Evans MJ, Kaufman MH. Establishment in culture of pluripotential cells from mouse embryos. Nature. 1981; 292:154–156. [PubMed: 7242681]
52. Martin GR. Isolation of a pluripotent cell line from early mouse embryos cultured in medium conditioned by teratocarcinoma stem cells. Proc Natl Acad Sci U S A. 1981; 78:7634–7638. [PubMed: 6950406]
53. Zvetkova I, Apedaile A, Ramsahoye B, Mermoud JE, Crompton LA, John R, et al. Global hypomethylation of the genome in XX embryonic stem cells. Nat Genet. 2005; 37:1274–1279. DOI: 10.1038/ng1663 [PubMed: 16244654]
54. Panning B, Dausman J, Jaenisch R. X chromosome inactivation is mediated by Xist RNA stabilization. Cell. 1997; 90:907–916. [PubMed: 9298902]
55. Naughton C, Sproul D, Hamilton C, Gilbert N. Analysis of active and inactive X chromosome architecture reveals the independent organization of 30 nm and large-scale chromatin structures. Mol Cell. 2010; 40:397–409. DOI: 10.1016/j.molcel.2010.10.013 [PubMed: 21070966]
56. Splinter E, de Wit E, Nora EP, Klous P, van de Werken HJG, Zhu Y, et al. The inactive X chromosome adopts a unique three-dimensional conformation that is dependent on Xist RNA. Genes Dev. 2011; 25:1371–1383. DOI: 10.1101/gad.633311 [PubMed: 21690198]
57. Wutz A, Rasmussen TP, Jaenisch R. Chromosomal silencing and localization are mediated by different domains of Xist RNA. Nat Genet. 2002; 30:167–174. DOI: 10.1038/ng820 [PubMed: 11780141]
58. Wutz A. Haploid mouse embryonic stem cells: rapid genetic screening and germline transmission. Annu Rev Cell Dev Biol. 2014; 30:705–722. DOI: 10.1146/annurev-cellbio-100913-012920 [PubMed: 25288120]
59. Monfort A, Di Minin G, Postlmayr A, Freimann R, Arieti F, Thore S, et al. Identification of Spen as a Crucial Factor for Xist Function through Forward Genetic Screening in Haploid Embryonic Stem Cells. Cell Rep. 2015; 12:554–561. DOI: 10.1016/j.celrep.2015.06.067 [PubMed: 26190100]
60. Brown CJ, Baldry SE. Evidence that heteronuclear proteins interact with XIST RNA in vitro. Somat Cell Mol Genet. 1996; 22:403–417. [PubMed: 9039849]
61. Royce-Tolland ME, Andersen AA, Koyfman HR, Talbot DJ, Wutz A, Tonks ID, et al. The A-repeat links ASF/SF2-dependent Xist RNA processing with random choice during X inactivation. Nat Struct Mol Biol. 2010; 17:948–954. DOI: 10.1038/nsmb.1877 [PubMed: 20657585]
62. Chu C, Qu K, Zhong FL, Artandi SE, Chang HY. Genomic maps of long noncoding RNA occupancy reveal principles of RNA-chromatin interactions. Mol Cell. 2011; 44:667–678. DOI: 10.1016/j.molcel.2011.08.027 [PubMed: 21963238]
63. Chu C, Zhang QC, da Rocha ST, Flynn RA, Bharadwaj M, Calabrese JM, et al. Systematic discovery of Xist RNA binding proteins. Cell. 2015; 161:404–416. DOI: 10.1016/j.cell.2015.03.025 [PubMed: 25843628]
64. Minajigi A, Froberg JE, Wei C, Sunwoo H, Kesner B, Colognori D, et al. Chromosomes. A comprehensive Xist interactome reveals cohesin repulsion and an RNA-directed chromosome conformation. Science. 2015; 349doi: 10.1126/science.aab2276
65. Simon MD, Pinter SF, Fang R, Sarma K, Rutenberg-Schoenberg M, Bowman SK, et al. High-resolution Xist binding maps reveal two-step spreading during X-chromosome inactivation. Nature. 2013; 504:465–469. DOI: 10.1038/nature12719 [PubMed: 24162848]
66. Buzin CH, Mann JR, Singer-Sam J. Quantitative RT-PCR assays show Xist RNA levels are low in mouse female adult tissue, embryos and embryoid bodies. Dev Camb Engl. 1994; 120:3529–3536.

67. Sunwoo H, Wu JY, Lee JT. The Xist RNA-PRC2 complex at 20-nm resolution reveals a low Xist stoichiometry and suggests a hit-and-run mechanism in mouse cells. Proc Natl Acad Sci U S A. 2015; 112:E4216–4225. DOI: 10.1073/pnas.1503690112 [PubMed: 26195790]
68. Smeets D, Markaki Y, Schmid VJ, Kraus F, Tattermusch A, Cerase A, et al. Three-dimensional super-resolution microscopy of the inactive X chromosome territory reveals a collapse of its active nuclear compartment harboring distinct Xist RNA foci. Epigenetics Chromatin. 2014; 7:8.doi: 10.1186/1756-8935-7-8 [PubMed: 25057298]
69. Guyochin A, Maenner S, Chu ET-J, Hentati A, Attia M, Avner P, et al. Live Cell Imaging of the Nascent Inactive X Chromosome during the Early Differentiation Process of Naive ES Cells towards Epiblast Stem Cells. PLoS ONE. 2014; 9:e116109.doi: 10.1371/journal.pone.0116109 [PubMed: 25546018]
70. Trapnell C. Defining cell types and states with single-cell genomics. Genome Res. 2015; 25:1491–1498. DOI: 10.1101/gr.190595.115 [PubMed: 26430159]
71. Dixon JR, Selvaraj S, Yue F, Kim A, Li Y, Shen Y, et al. Topological domains in mammalian genomes identified by analysis of chromatin interactions. Nature. 2012; 485:376–380. DOI: 10.1038/nature11082 [PubMed: 22495300]
72. Lieberman-Aiden E, van Berkum NL, Williams L, Imakaev M, Ragoczy T, Telling A, et al. Comprehensive mapping of long-range interactions reveals folding principles of the human genome. Science. 2009; 326:289–293. DOI: 10.1126/science.1181369 [PubMed: 19815776]
73. Marks H, Kerstens HHD, Barakat TS, Splinter E, Dirks RAM, van Mierlo G, et al. Dynamics of gene silencing during X inactivation using allele-specific RNA-seq. Genome Biol. 2015; 16:149.doi: 10.1186/s13059-015-0698-x [PubMed: 26235224]
74. Moindrot B, Cerase A, Coker H, Masui O, Grijzenhout A, Pintacuda G, et al. A Pooled shRNA Screen Identifies Rbm15, Spen, and Wtap as Factors Required for Xist RNA-Mediated Silencing. Cell Rep. 2015; 12:562–572. DOI: 10.1016/j.celrep.2015.06.053 [PubMed: 26190105]
75. Hasegawa Y, Brockdorff N, Kawano S, Tsutui K, Tsutui K, Nakagawa S. The matrix protein hnRNP U is required for chromosomal localization of Xist RNA. Dev Cell. 2010; 19:469–476. DOI: 10.1016/j.devcel.2010.08.006 [PubMed: 20833368]
76. Helbig R, Fackelmayer FO. Scaffold attachment factor A (SAF-A) is concentrated in inactive X chromosome territories through its RGG domain. Chromosoma. 2003; 112:173–182. DOI: 10.1007/s00412-003-0258-0 [PubMed: 14608463]
77. Pullirsch D, Härtel R, Kishimoto H, Leeb M, Steiner G, Wutz A. The Trithorax group protein Ash2l and Saf-A are recruited to the inactive X chromosome at the onset of stable X inactivation. Dev Camb Engl. 2010; 137:935–943. DOI: 10.1242/dev.035956
78. Hasegawa Y, Brockdorff N, Kawano S, Tsutui K, Tsutui K, Nakagawa S. The matrix protein hnRNP U is required for chromosomal localization of Xist RNA. Dev Cell. 2010; 19:469–476. DOI: 10.1016/j.devcel.2010.08.006 [PubMed: 20833368]
79. Yamada N, Hasegawa Y, Yue M, Hamada T, Nakagawa S, Ogawa Y. Xist Exon 7 Contributes to the Stable Localization of Xist RNA on the Inactive X-Chromosome. PLoS Genet. 2015; 11:e1005430.doi: 10.1371/journal.pgen.1005430 [PubMed: 26244333]
80. Hall LL, Carone DM, Gomez AV, Kolpa HJ, Byron M, Mehta N, et al. Stable C0T-1 repeat RNA is abundant and is associated with euchromatic interphase chromosomes. Cell. 2014; 156:907–919. DOI: 10.1016/j.cell.2014.01.042 [PubMed: 24581492]
81. Jeon Y, Lee JT. YY1 tethers Xist RNA to the inactive X nucleation center. Cell. 2011; 146:119–133. DOI: 10.1016/j.cell.2011.06.026 [PubMed: 21729784]
82. Hong YK, Ontiveros SD, Strauss WM. A revision of the human XIST gene organization and structural comparison with mouse Xist. Mamm Genome Off J Int Mamm Genome Soc. 2000; 11:220–224.
83. Sigova AA, Abraham BJ, Ji X, Molinie B, Hannett NM, Guo YE, et al. Transcription factor trapping by RNA in gene regulatory elements. Science. 2015; 350:978–981. DOI: 10.1126/science.aad3346 [PubMed: 26516199]
84. Petersen M, Wengel J. LNA: a versatile tool for therapeutics and genomics. Trends Biotechnol. 2003; 21:74–81. DOI: 10.1016/S0167-7799(02)00038-0 [PubMed: 12573856]

85. Sarma K, Levasseur P, Aristarkhov A, Lee JT. Locked nucleic acids (LNAs) reveal sequence requirements and kinetics of Xist RNA localization to the X chromosome. Proc Natl Acad Sci U S A. 2010; 107:22196–22201. DOI: 10.1073/pnas.1009785107 [PubMed: 21135235]

86. Barr ML, Bertram EG. A morphological distinction between neurones of the male and female, and the behaviour of the nucleolar satellite during accelerated nucleoprotein synthesis. Nature. 1949; 163:676. [PubMed: 18120749]

87. Forsberg JG, Lindh J. Sex chromatin in adult and foetal rat. Nature. 1962; 195:1329. [PubMed: 13958789]

88. Moore KL, Barr ML. Morphology of the nerve cell nucleus in mammals, with special reference to the sex chromatin. J Comp Neurol. 1953; 98:213–231. [PubMed: 13052743]

89. Ohno S, Kaplan WD, Kinosita R. Somatic association of the positively heteropycnotic x-chromosomes in female mice (Mus musculus). Exp Cell Res. 1958; 15:616–618. [PubMed: 13609640]

90. Ohno S, Kovacs ET, Kinosita R. On the X-chromosomes of mouse mammary carcinoma cells. Exp Cell Res. 1959; 16:462–465. [PubMed: 13653016]

91. Ohno S, Hauschka TS. Allocycly of the X-chromosome in tumors and normal tissues. Cancer Res. 1960; 20:541–545. [PubMed: 14428472]

92. Ohno S, Kaplan WD, Kinosita R. On the end-to-end association of the X and Y chromosomes of Mus musculus. Exp Cell Res. 1959; 18:282–290. [PubMed: 14428476]

93. Lyon MF. Gene action in the X-chromosome of the mouse (Mus musculus L.). Nature. 1961; 190:372–373. [PubMed: 13764598]

94. Bischoff A, Albers J, Kharboush I, Stelzer E, Cremer T, Cremer C. Differences of size and shape of active and inactive X-chromosome domains in human amniotic fluid cell nuclei. Microsc Res Tech. 1993; 25:68–77. DOI: 10.1002/jemt.1070250110 [PubMed: 8353309]

95. Rinke B, Bischoff A, Meffert M-C, Scharschmidt R, Hausmann M, Stelzer E, et al. Volume ratios of painted chromosome territories 5, 7 and X in female human cell nuclei studied with confocal laser microscopy and the Cavalieri estimator. Bioimaging. 1995; 3

96. Bolland DJ, King MR, Reik W, Corcoran AE, Krueger C. Robust 3D DNA FISH using directly labeled probes. J Vis Exp JoVE. 2013; doi: 10.3791/50587

97. Chaumeil J, Augui S, Chow JC, Heard E. Combined immunofluorescence, RNA fluorescent in situ hybridization, and DNA fluorescent in situ hybridization to study chromatin changes, transcriptional activity, nuclear organization, and X-chromosome inactivation. Methods Mol Biol Clifton NJ. 2008; 463:297–308. DOI: 10.1007/978-1-59745-406-3_18

98. Markaki Y, Smeets D, Cremer M, Schermelleh L. Fluorescence in situ hybridization applications for super-resolution 3D structured illumination microscopy. Methods Mol Biol Clifton NJ. 2013; 950:43–64. DOI: 10.1007/978-1-62703-137-0_4

99. Teller K, Illner D, Thamm S, Casas-Delucchi CS, Versteeg R, Indemans M, et al. A top-down analysis of Xa- and Xi-territories reveals differences of higher order structure at ≥ 20 Mb genomic length scales. Nucl Austin Tex. 2011; 2:465–477. DOI: 10.4161/nucl.2.5.17862

100. Zhu P, Li G. Structural insights of nucleosome and the 30-nm chromatin fiber. Curr Opin Struct Biol. 2016; 36:106–115. DOI: 10.1016/j.sbi.2016.01.013 [PubMed: 26872330]

101. Tremethick DJ. Higher-order structures of chromatin: the elusive 30 nm fiber. Cell. 2007; 128:651–654. DOI: 10.1016/j.cell.2007.02.008 [PubMed: 17320503]

102. Greulich KO, Wachtel E, Ausio J, Seger D, Eisenberg H. Transition of chromatin from the “10 nm” lower order structure, to the “30 nm” higher order structure as followed by small angle X-ray scattering. J Mol Biol. 1987; 193:709–721. [PubMed: 3612790]

103. Maeshima K, Imai R, Tamura S, Nozaki T. Chromatin as dynamic 10-nm fibers. Chromosoma. 2014; 123:225–237. DOI: 10.1007/s00412-014-0460-2 [PubMed: 24737122]

104. Gilbert N, Boyle S, Fiegler H, Woodfine K, Carter NP, Bickmore WA. Chromatin architecture of the human genome: gene-rich domains are enriched in open chromatin fibers. Cell. 2004; 118:555–566. DOI: 10.1016/j.cell.2004.08.011 [PubMed: 15339661]

105. Syvänen A-C. Accessing genetic variation: genotyping single nucleotide polymorphisms. Nat Rev Genet. 2001; 2:930–942. DOI: 10.1038/35103535 [PubMed: 11733746]

106. Denholtz M, Bonora G, Chronis C, Splinter E, de Laat W, Ernst J, et al. Long-range chromatin contacts in embryonic stem cells reveal a role for pluripotency factors and polycomb proteins in genome organization. Cell Stem Cell. 2013; 13:602–616. DOI: 10.1016/j.stem.2013.08.013 [PubMed: 24035354]

107. Rao SSP, Huntley MH, Durand NC, Stamenova EK, Bochkov ID, Robinson JT, et al. A 3D map of the human genome at kilobase resolution reveals principles of chromatin looping. Cell. 2014; 159:1665–1680. DOI: 10.1016/j.cell.2014.11.021 [PubMed: 25497547]

108. Rego A, Sinclair PB, Tao W, Kireev I, Belmont AS. The facultative heterochromatin of the inactive X chromosome has a distinctive condensed ultrastructure. J Cell Sci. 2008; 121:1119–1127. DOI: 10.1242/jcs.026104 [PubMed: 18334550]

109. Dekker J, Marti-Renom MA, Mirny LA. Exploring the three-dimensional organization of genomes: interpreting chromatin interaction data. Nat Rev Genet. 2013; 14:390–403. DOI: 10.1038/nrg3454 [PubMed: 23657480]

110. Deng X, Ma W, Ramani V, Hill A, Yang F, Ay F, et al. Bipartite structure of the inactive mouse X chromosome. Genome Biol. 2015; 16:152.doi: 10.1186/s13059-015-0728-8 [PubMed: 26248554]

111. Nora EP, Lajoie BR, Schulz EG, Giorgetti L, Okamoto I, Servant N, et al. Spatial partitioning of the regulatory landscape of the X-inactivation centre. Nature. 2012; 485:381–385. DOI: 10.1038/nature11049 [PubMed: 22495304]

112. Giacalone J, Friedes J, Francke U. A novel GC-rich human macrosatellite VNTR in Xq24 is differentially methylated on active and inactive X chromosomes. Nat Genet. 1992; 1:137–143. DOI: 10.1038/ng0592-137 [PubMed: 1302007]

113. Horakova AH, Moseley SC, McLaughlin CR, Tremblay DC, Chadwick BP. The macrosatellite DXZ4 mediates CTCF-dependent long-range intrachromosomal interactions on the human inactive X chromosome. Hum Mol Genet. 2012; 21:4367–4377. DOI: 10.1093/hmg/dds270 [PubMed: 22791747]

114. Ong C-T, Corces VG. CTCF: an architectural protein bridging genome topology and function. Nat Rev Genet. 2014; 15:234–246. DOI: 10.1038/nrg3663 [PubMed: 24614316]

115. Chadwick BP. DXZ4 chromatin adopts an opposing conformation to that of the surrounding chromosome and acquires a novel inactive X-specific role involving CTCF and antisense transcripts. Genome Res. 2008; 18:1259–1269. DOI: 10.1101/gr.075713.107 [PubMed: 18456864]

A

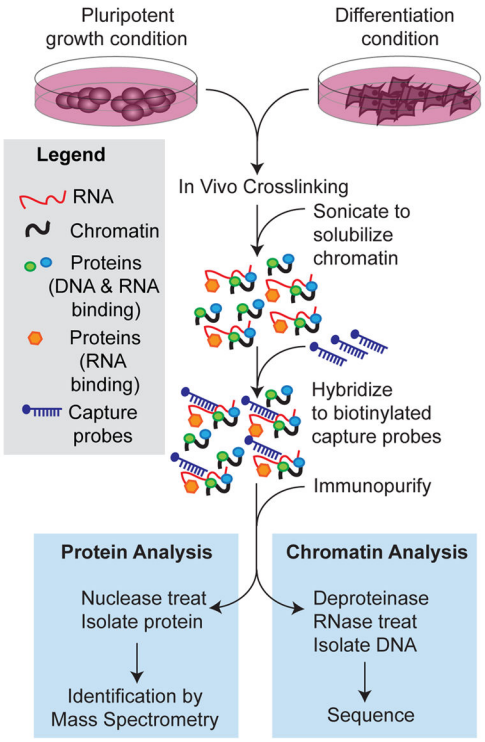

B

Parameter	RAP-seq	CHART-seq	ChIRP-seq
Fixation	DSG 3% FA	1% FA	1% GA or 3% FA
DNA Fragmentation	Sonication & DNase	Sonication	Sonication
Capture Probe Length (nt)	120	22-28	20
Probe type	RNA or DNA	DNA	DNA
Probe distribution	Tiled with a 15nt overlap	1 probe per 300-500nt	1 probe per 100nt
Targeted region	Complete Xist RNA	Complete Xist RNA	N/A
Hybridization conditions	Tris Buffered solution with: Na Deoxycholate SDS NP40 LiCl Guanidine Iso-thiocyanate	HEPES Buffered solution with: Denhards sol'n SDS Sarkosyl	Tris Buffered solution with: SDS Formamide
Adapted for Mass Spectrometry	Yes	Yes	Yes
Cell types used for *Xist* RNA analysis	- Mouse Lung Fibroblasts - Differentiated female ESCs (6h) - Inducible male ESCs (0-6h dox)	- Mouse Embryonic Fibroblasts - female ESCs differentiated for 3 and 7 days	N/A

Figure 1. A general overview of the protocols used for the purification of RNA-Chromatin complexes by RAP, CHART, and ChIRP

(A) RNA-expressing cells (For *Xist* RNA, these include female somatic cells such as MEFs or ESCs induced to express *Xist* either through differentiation or treatment with doxycycline if using cells harboring a tetracycline-inducible *Xist* transgene) are crosslinked using formaldehyde (CHART), Disuccinimidyl Glutarate/formaldehyde (RAP), and glutaraldehyde or formaldehyde (ChIRP). Chromatin is solubilized by sonication with (RAP) or without (CHART/ChIRP) DNase treatment. After incubation of the fragmented chromatin lysate with pooled biotinylated oligos antisense to the target RNA, oligos are immunopurified using streptavidin beads to isolate captured RNA-chromatin complexes. When studying the chromatin targeting of RNAs, the RNA isolates are reverse-crosslinked and deproteinated by treatment with proteinase K. Any remaining RNA is degraded by incubation of the lysate with RNase prior to purification of the selected DNA for high-throughput sequencing library preparation to identify the regions of chromatin targeted by the RNA of interest. This approach can also be used to isolate the protein components of RNA chromatin complexes if the captured lysates are treated with nucleases rather than a protease. **(B)** Table listing the main experimental variables that differ between RAP, ChIRP, and CHART, and their application to studies of *Xist* RNA.

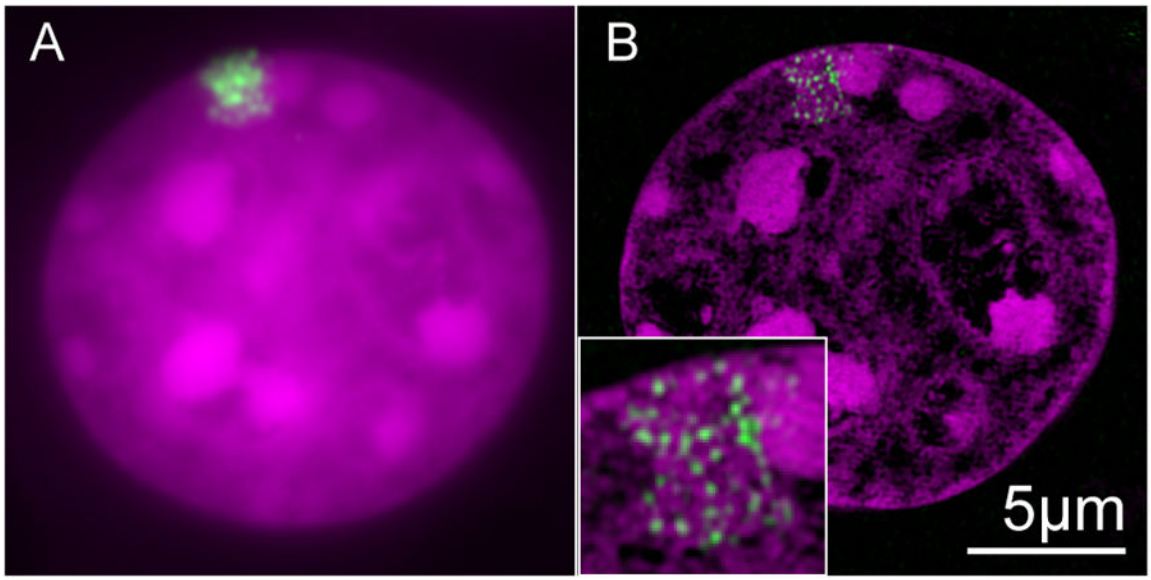

Image courtesy of Dr. Yolanda Markaki

Figure 2. The *Xist* RNA cloud is composed of discrete RNA foci distributed throughout the Xi territory

(A) A Representative epifluorescent micrograph of the RNA FISH signal (green) obtained using DNA probes against the full length *Xist* RNA in mouse C127 cells, stained with DAPI (purple). **(B)** Same as (A) except in this experiment cells were imaged with super resolution 3D-Structured Illumination Microscopy. Inset: Magnification of the *Xist* RNA signal.

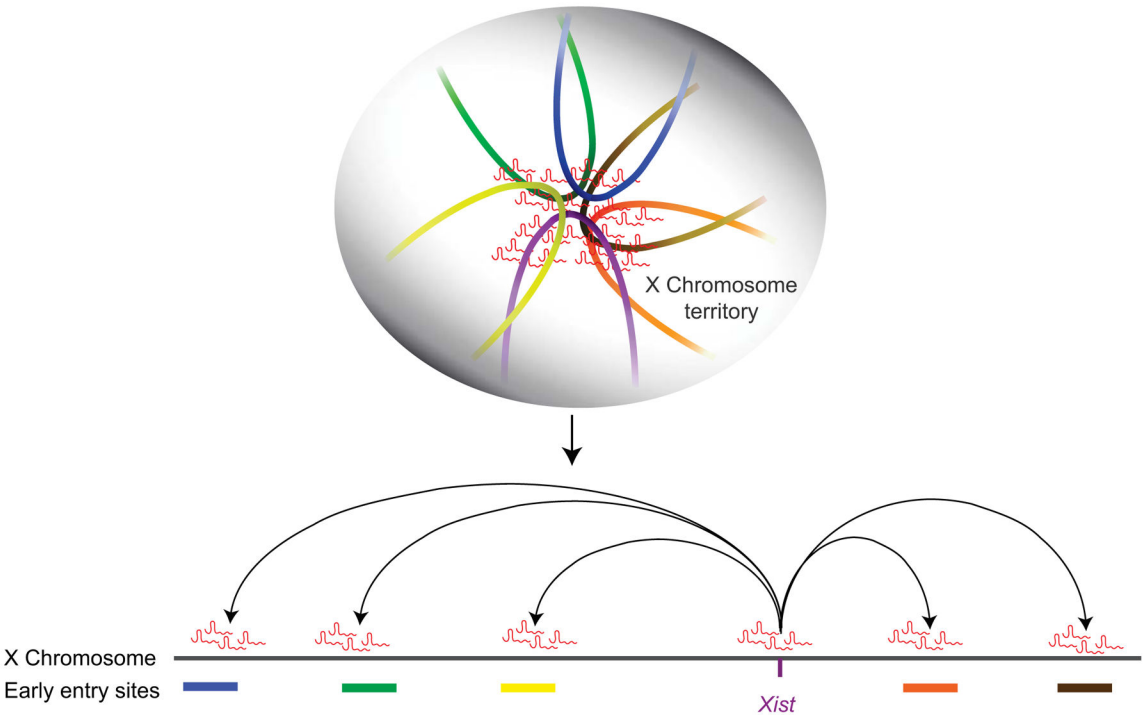

Figure 3. The *Xist* RNA spreads across the X-chromosome by transferring to genomic locations in close spatial proximity to the *Xist* locus during the onset of XCI

Within a few hours of its initial expression, *Xist* RNA transfers to genomic sites in close 3D proximity to the genomic *Xist* locus. These early entry sites, when mapped to a linear representation of the X chromosome, assume discrete locations that are distributed across the length of the chromosome. The entry sites and 3D maps are not drawn to scale and are not representative of the number, size or location of the early entry sites on the X. The image simply illustrates the concept of proximity-mediated transfer of *Xist* RNA over the X chromosome as defined in Engreitz et al., 2013.

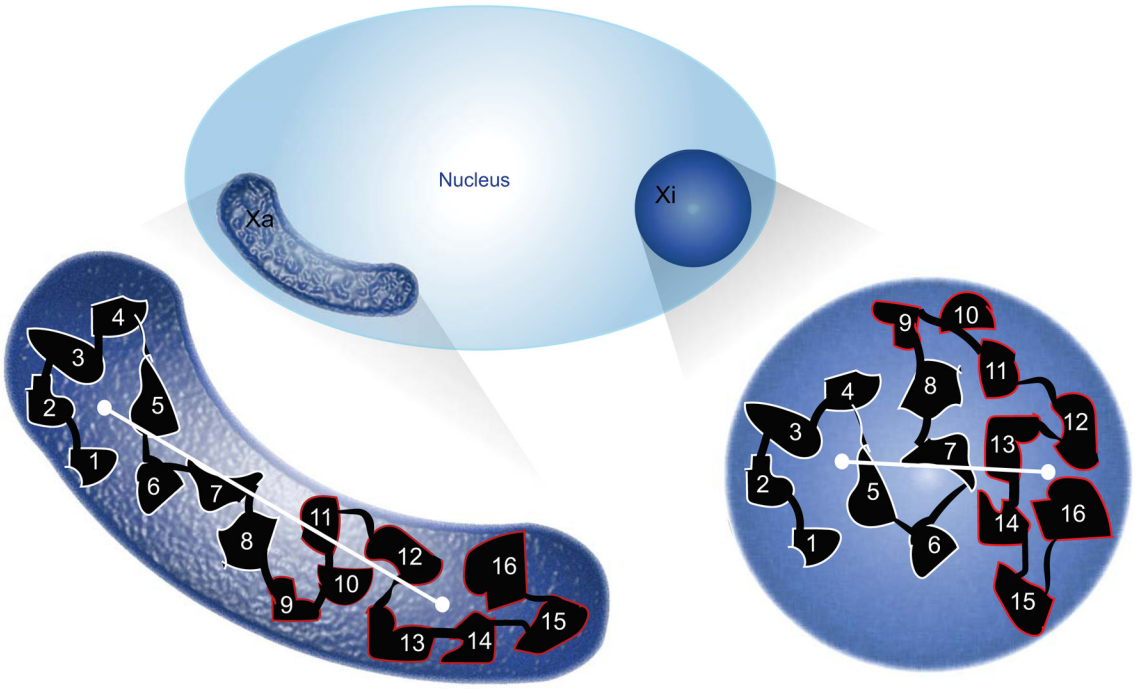

Figure 4. The shape and chromatin organization of the Xi is distinct from that of the Xa

The inactive X chromosome adopts a smoother, more spherical shape than the Xa, which tends to be more ellipsoid with a more irregular surface area (not drawn to scale). The enlarged Xi and Xa chromosomes each contain a representation of two large chromosomal segments (red and white outlined regions) that differ in their relative arrangement but not in their compaction. Sample intersegment distances (ISDs) are depicted as white lines and illustrate how changes in overall domain architecture of the Xi relative to the Xa can alter ISD measurements at the multi-Mb scale but that ISDs between single or sub-Mb domains (region labeled 1–16) remain unchanged. Images adapted from Teller et al., 2011.